Journal of Materials Research and Technology 39 (2025) 5238–5250

Contents lists available at ScienceDirect

Journal of Materials Research and Technology

journal homepage: www.elsevier.com/locate/jmrt

Synergistic Akermanite/PMMA/Zirconia Composites with Nature Inspired Structure via 3D Printing for orthopaedics

M. Girija [a,b], T. Sampath Kumar [a,*], Sumsun Naher [c]

[a] School of Mechanical Engineering, Vellore Institute of Technology, Vellore, Tamil Nadu, India
[b] Department of Mechanical Engineering, Indian Institute of Technology Madras, India
[c] Department of Engineering, School of Science & Technology (SST), City St George's, University of London, London, UK

ARTICLE INFO

Keywords:
Akermanite
PMMA
Zirconia
Bio plotter
Additive manufacturing
Bone scaffold
Orthopaedic applications

ABSTRACT

The development of orthopedic implants requires bone cements that combine bioactivity with mechanical stability. In this study, 25% Akermanite/PMMA/25% Zirconia composites were fabricated using a bio plotter additive manufacturing process in three structural configurations, solid, 5-channel, and 6-channel–mimicking the lotus root's porous structure. Structural and biological characterizations were conducted using SEM, micro-CT, mechanical testing, antibacterial assays, and hemocompatibility and cytocompatibility analyses. SEM confirmed uniform phase dispersion and strong interfacial bonding, while micro-CT revealed porosities of 53 ± 1 % (5-channel) and 67 ± 3 % (6-channel). The 6-channel design exhibited superior antibacterial activity against *E. coli* (16 mm) and *S. aureus* (21 mm), higher cell viability, and the lowest hemolytic effect. Compressive strengths were 145.6 MPa (solid), 132.8 MPa (5-channel), and 120.5 MPa (6-channel), demonstrating a balance between porosity and strength. Overall, the 6-channel structure achieved an optimal trade-off between mechanical performance and biological functionality, suggesting its potential for next-generation orthopedic applications.

1. Introduction

A major subcategory of additive manufacturing (AM) referred to as 3-D printing has transformed the field of biomedical engineering via printing of anatomically complex and invaluable multifunctional implants and scaffolds that are patient specific. More than any conventional manufacturing process, AM provides exceptional levels of design freedom [1]precision and enable mechanical and biological properties to be tailored to meet a specific clinical need which is of critical importance in orthopaedics. Structural design parameters such as pore size, porosity, and interconnectivity are key to optimizing scaffolds for bone tissue regeneration [2]. These parameters affect not only mechanical strength but also cell migration, vascularization, and new bone ingrowth [3]. Despite the success of conventional sponge-like scaffolds, limitations such as isotropic stress distribution and the bottle-neck effect where small interconnections between macropores hinder deep tissue infiltration remain unresolved [4]. The sponge-like scaffolds show isotropic stress transmission, which could hinder their integration with the host bone, in contrast to the anisotropy of true bone. Spiro S et al. [4] found the anisotropic porous structures in bio ceramics were prepared using natural wood or fibres as a sporogen, and anisotropic biomaterials with good pore connectivity have recently received a lot of attention to the research. To overcome these constraints, researchers are increasingly turning to anisotropic and biomimetic structures inspired by natural geometries. A promising biomimetic design is the lotus-root-like multichannel scaffold, which mimics the natural hollow structure of lotus roots. These structures provide high porosity, low flow resistance, and superior gas/nutrient exchange, making them ideal for promoting angiogenesis and osteogenesis [5]. Vascularization is crucial to the formation of new bones. Blood vessels developed from endothelial cells that forms microtubes. Study has shown that endothelial cells can form rudimentary vasculature in vitro using a microfluidic system, which includes microchannels [6]. This design allows for control over the degradation of the polymer scaffold, ensuring that it degrades at a rate that is compatible with the sintering process of porous ceramics [7]. Research suggests that using 3D scaffolds to incorporate parts of channels can improve oxygen and nutrient perfusion and promote tissue growth. Materials with lotus root-like structures (multichannel) may have higher angiogenic and osteogenic bioactivity for large bone regeneration [8]. Preliminary research has demonstrated the benefits of

* Corresponding author.
E-mail addresses: girija.m2020@vitstudent.ac.in (M. Girija), sampath.thepperumal@vit.ac.in (T. Sampath Kumar), Sumsun.Naher.1@citystgeorges.ac.uk (S. Naher).

https://doi.org/10.1016/j.jmrt.2025.10.152
Received 2 September 2025; Received in revised form 14 October 2025; Accepted 19 October 2025
Available online 20 October 2025

2-, 3-, and 4-channel scaffolds in enhancing cell infiltration and vascularization. However, the systematic fabrication and evaluation of five- and six-channel lotus-root-inspired scaffolds remain largely unexplored [9]. Additive manufacturing, especially with polymer and ceramic composites for the biomedical application, plays a very important role in biomedical fields. Bio Plotter is a technology used for modeling scaffolds for tissue engineering and organ printing [10]. It can use various materials like ceramic pastes (Hydroxyapatite and Tricalcium Phosphate) for porous bone scaffolds, bioresorbable polymers for drug delivery, and agar, gelatine, chitosan, collagen, alginate, and fibrin as carriers for cells used in organ printing [11]. Orthopaedic requirements would require material properties to guarantee mechanical performance of the implant, prostheses, fixation devices, safety, and life, as well as compatibility with the human body. Polymethyl methacrylate (PMMA) is one of the most common biocompatible materials due to the favourable processing properties of this type of polymer and sufficient mechanical properties to be used in orthopaedic applications [12,13]. However, the brittleness in its nature, as well as low biological activity, does not allow the material to perform well in the long term with regards to load bearing and osseointegration. Our previous studies presented by us confirm that reinforcement of the PMMA with bioactive ceramics, especially with akermanite-($Ca_2MgSi_2O_7$-AKT) and zirconia (ZrO_2) would substantially increase the mechanical strength, the bioactivity and increased integration with the bones [14]. These composites enhance better osteointegration, higher toughness and reduce loosening of implants with time thus making them great prospects in orthopaedic practice as advanced bone cements.

Additionally, the 3D bioplotter offers advanced capabilities for printing multi-material, multi-channel scaffolds using polymers and ceramic composites in sterile environments. This method allows natural bone, thereby supporting both mechanical integration and biological regeneration [15]. This technology is part of the additive manufacturing group, Envision Tec has developed a commercial 3D bioplotter technology, invented at the Freiburg Materials Research Centre in 1999 [16]. This system allows for the printing of biological cells and various biomaterials, including living cells. It is designed for use in sterile environments for bio-fabrication and clinically relevant soft tissue grafts [17]. The biomaterials can be melted or dissolved, and then dispensed layer-by-layer on a collecting plate or liquid medium. The method involves deposition of materials in three dimensions using air or mechanical pressure [18]. This innovative approach opens up new possibilities for the fabrication of advanced composite materials [19]. This structure closely mimics the natural porosity of bone, providing interconnected channels that enhance cell migration, nutrient transport, and vascularization, all of which are critical for successful bone tissue engineering, ensuring a balance between structural integrity and optimal cell migration and proliferation. Previous researchers have investigated lotus-root and other biomimetic channel scaffolds, although most have only considered a smaller number of channels with single material in this work, however, this novel approach provide a composite of materials offers an excellent match of bioactivity (ion release of akermanite), structural reinforcement (zirconia) and printability (PMMA). This allows the creation of 5- and 6-channel lotus-stem structures that remain strong despite the fact that they contain holes in them that support bone growth [20].

The objective of this study is to discover the preparation and properties of the lotus root-like biomimetic materials in tissue engineering in comparison with traditional 3D scaffolds for cell delivery and tissue regeneration. By combining the biocompatibility of polymers with the mechanical strength and osteoconductivity of ceramics, this composite approach enables the creation of bioactive scaffolds that closely resemble the hierarchical structure of natural cortical bone, 25% AKT/PMMA/25% ZrO_2 composites fabricated via bioplotter-based additive manufacturing. This gap motivates the present work, which aims to elucidate how such biomimetic internal designs affect the composite's structural and biological performance. Despite progress, critical knowledge gaps persist regarding the influence of channel number on mechanical strength, cellular response, vascularization, and nutrient diffusion. Addressing these gaps is crucial for optimizing scaffold design for large bone defect repair and clinical translation.

2. Materials and methods

2.1. Source of materials

2.1.1. Akermanite (AKT) preparation

The components that were obtained from Avra Synthesis Private Limited were TEOS, which stands for tetraethyl orthosilicate, calcium nitrate tetrahydrate, which is Ca $(NO_3)_24H_2O$, and magnesium nitrate hexahydrate, which is Mg $(NO_3)_2.6H_2O$. Sigma Alrich supplied nitric acid (HNO_3), magnesium oxide (MgO), silicon dioxide (SiO_2), and calcium oxide (CaO). All of these chemicals were utilized to prepare AKT samples. The chemicals obtained have a purity of 98 %. The AKT synthesis process proceeded according to our earlier research [21], followed by Sol-gel and ball mil Combined process with supplemental heat treatment.

2.1.2. PMMA/zirconia

PMMA powder have been purchased from TCI chemicals Chennai and ZrO_2 powder were purchased from Avra Synthesis Private Limited.

2.1.3. Live/dead cell viability assay

Live/dead cell viability was assessed using. A staining solution containing 2 μM Calcein-AM (to stain live cells green) and 4 μM Ethidium Homodimer-1 (to stain dead cells red) in PBS was prepared and added to each well.

2.1.4. Bacteria

The bacteria employed for antibacterial activity were *Escherichia coli* - (*E. coli*) and *Staphylococcus aureus* - (*S. aureus*), which were obtained from the Coimbatore Medical College and Hospital (CMHC), Department of Microbiology. In Potato dextrose agar (PDA) and nutrient agar medium, the bacterial and fungal cultures were maintained.

2.2. Fabrication method

2.2.1. Preparation of bio-ink

The 25% AKT/PMMA/25% ZrO_2 composite was created by combining 2g of PMMA content 50 wt% powder matrix, 1g of, and 1g of ZrO_2 which made the total filler content 50 wt% (25wt% AKT + 25wt% ZrO_2), 1 mL of liquid methyl methacrylate (MMA) was added to these solid powders and left to polymerize in place to create the cured PMMA matrix. This enables a tight control of the ceramic-to-polymer ratio with the end product having uniformly dispersed solids of 50 % in the PMMA, based on our previous formulation indicated a liquid to-powder. The (powder: liquid) phase was prepared by mixing composite powder with methyl methacrylate (MMA) monomer at a 2:1 (powder: liquid) ratio. (L/P) ratio of the mixture was 0.33, which is the ratio of MMA to total solids. This extensive formulation provides reproducibility of the composite formulation. The mixture was then gradually incorporated into the paste under continuous mixing to obtain a homogeneous viscous slurry with suitable rheological properties for 3D printing. Depicted in Fig. 1.

The ink is loaded into a sterilized syringe compatible with the 3D Bioplotter, and the bioplotter is calibrated to set process parameters such as extrusion pressure (0.7 bar), nozzle speed (10 mm/s), and temperature (22 °C) to obtain the lotus root structure of scaffold. The substrate is prepared for printing by cleaning with ethanol or deionized water and ensuring it is flat and secure in the bioplotter stage. The final inspection involves inspecting the material consistency, viscosity, and homogeneity before starting the printing process and performing a test extrusion to validate flow characteristics [22]. The ink formulation is

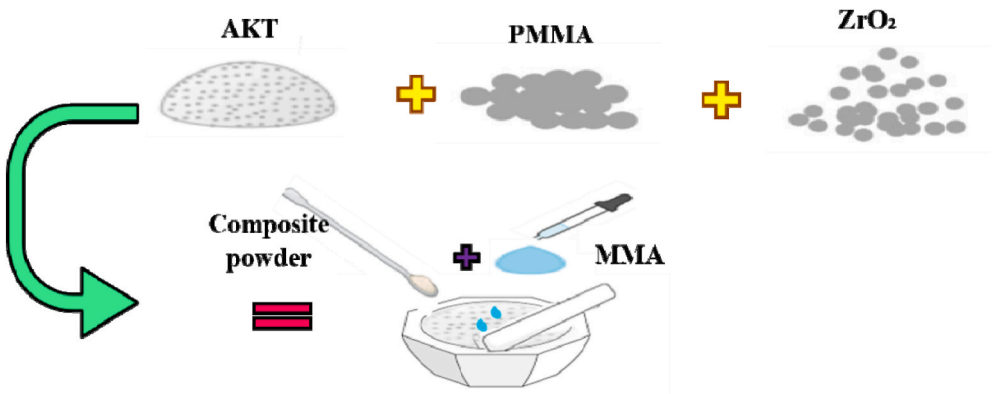

Fig. 1. Preparing steps of the AKT/PMMA/ZrO_2 composite in the form of viscous bio-ink.

adjusted based on preliminary tests to achieve desired print fidelity.

Furthermore, rheological analysis of the composite designed for the lotus root structure with distinct internal designs (5- and 6-channel) created utilizing the Bioplotter additive manufacturing technique was carried out to assess printability and flow stability. The viscosity vs shear rate graph showed in Fig. 2, strong shear-thinning behavior, with viscosity decreasing dramatically with increasing shear rate, indicating that the paste is suitable for extrusion-based printing. At low shear rates ($<10\ s^{-1}$), the viscosity remained reasonably high, retaining structural integrity following deposition. At higher shear rates ($>100\ s^{-1}$), the viscosity reduced dramatically, allowing for smooth flow through the nozzle. The recovery versus time curve showed remarkable thixotropic recovery, with more than 90 % viscosity restored within 10 s of shear cessation, indicating the material's capacity to regain its form and sustain succeeding layers without collapse. These rheological parameters confirmed that this combination is suitable for establishing complex lotus stem-inspired designs with well-defined channel geometries and layer fidelity utilizing the Bioplotter AM technique.

2.2.2. Fabrication of lotus root-inspired scaffold

The solid structure (Ss) was designed with a CAD-specified diameter of 4 mm, and the as-printed measurement showed a diameter of 3.98 ± 0.03 mm, indicating high fidelity to the design. For the 5-channel structure (5C), the cylinders were designed with a diameter of 4 mm and a height of 15 mm, with each channel having a diagonal of 350 μm. The as-printed cylinders measured 3.94 ± 0.04 mm in diameter and 14.92 ± 0.06 mm in height, while the channel diagonals measured 345 ± 5 μm. Dimensional tolerances were ±0.05 mm for the cylinder and ±5 μm for the channels, demonstrating close agreement with the CAD specifications. Similarly, for the 6-channel structure (6C), the cylinders were designed with a diameter of 4 mm, a height of 15 mm, and channel diagonals of 300 μm. The as-printed measurements showed a cylinder diameter of 3.98 ± 0.02 mm, a height of 14.92 ± 0.06 mm, and channel diagonals of 298 ± 5 μm, again indicating excellent correspondence between the CAD design and printed structures. The 3D CAD modes are shown in Fig. 3.

Fabrication of Structures Lotus root-inspired structures with solid, 5-channel, and 6-channel configurations were fabricated using a Bioplotter additive manufacturing system (EnvisionTEC), which is shown in Fig. 3(a). The material composition comprised 25%AKT/PMMA/25% ZrO_2 powder with liquid MMA The paste was loaded into the bio plotter's extrusion system and printed layer-by-layer following predefined CAD designs for the geometries. The fabricated samples are shown in Fig. 4(b).

2.3. Characterization of lotus root structure scaffold

2.3.1. Surface morphology

Field Emission Scanning Electron Microscopy (FESEM) analysis was conducted using a high-resolution scanning electron microscope (Model: Thermo Fisher FEI QUANTA 250 FEG), Field Emission Scanning Electron microscopy was used to study the micro structures. The 20 kV acceleration voltage was set for the analysis. The study examined the integrity, interfacial gaps, porosity distribution, and bonding between channel (5-channel and 6-channel) structures, evaluating structural reliability through microcracks, voids, or delamination, and assessing the dispersion of AKT and ZrO_2 particles within the PMMA matrix.

2.3.2. Micro-CT analysis

The printed structures underwent Micro-CT analysis to examine their internal porosity, and channel integrity. The scans were conducted using Micro-CT system (Model: Sky Scan 1273), under specific conditions

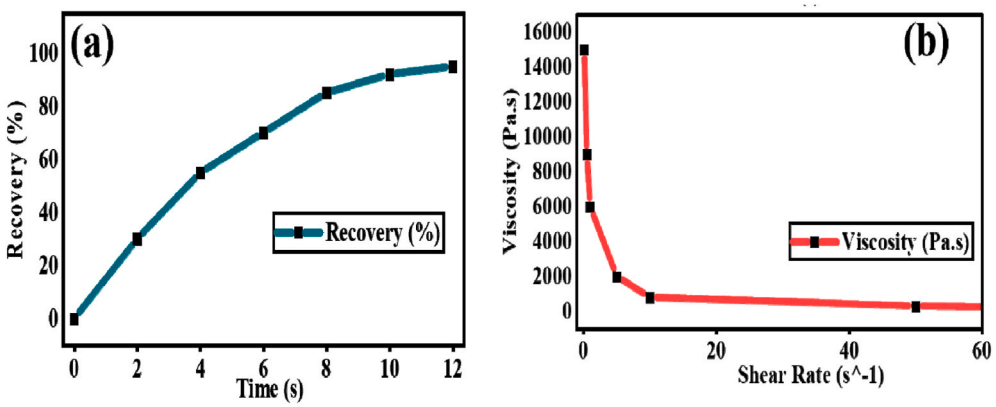

Fig. 2. Rheological characterization: (a) Recovery curve (b) Viscosity as a function of shear rate.

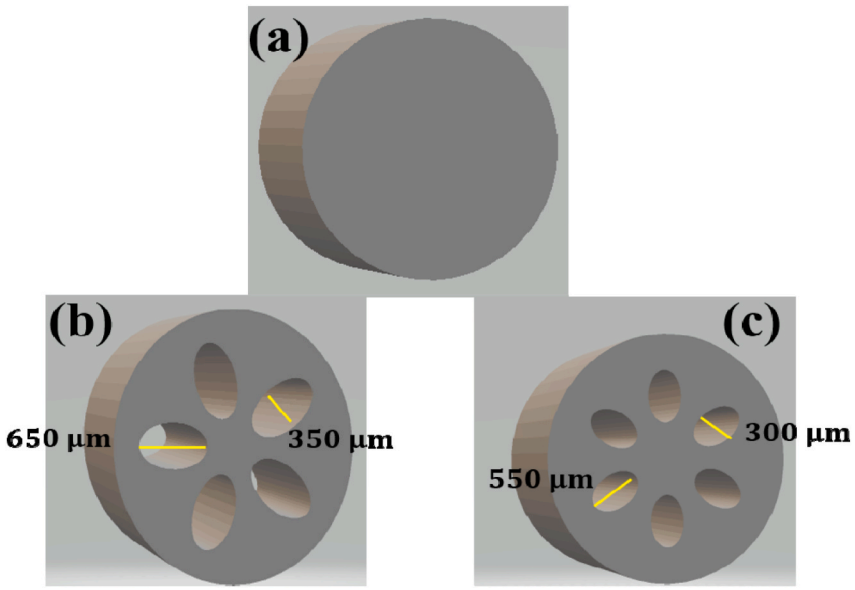

Fig. 3. 3D CAD models **(a)** solid structure **(b)** 5-channel structure, and **(c)** 6-channel structure.

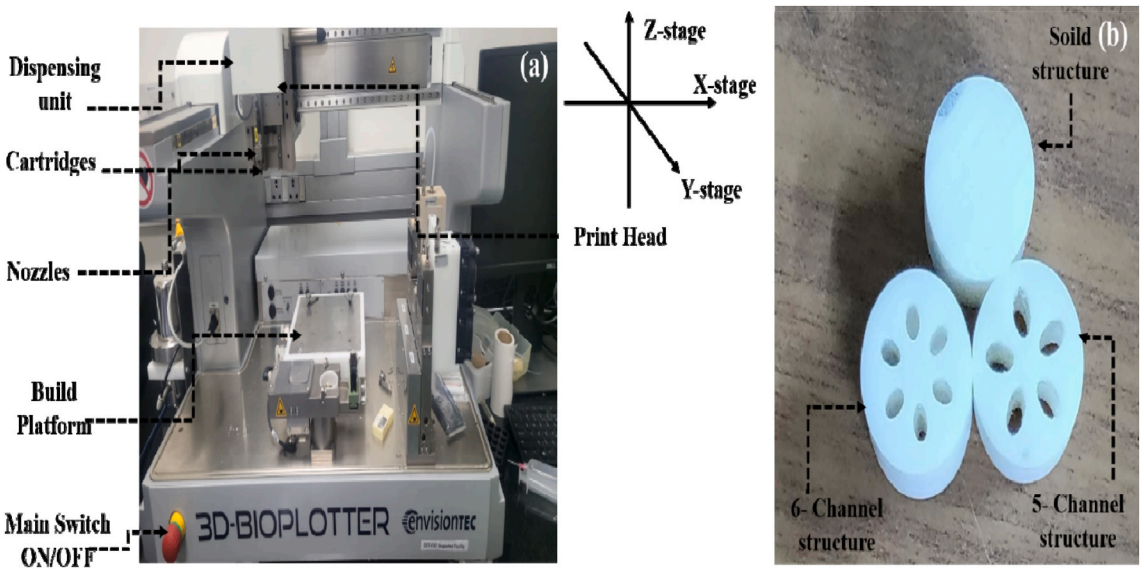

Fig. 4. **(a)** Bioplotter additive manufacturing system (Envision TEC), **(b)** Fabricated samples.

which includes an x-ray source of 80 kVp and 800 µA with 13.42 µm camera pixels. The lotus root structures were scanned and analysed using Micro-CT data in varying quantities using a CCD detector with 6.5 µm pixels and a copper filter of 0.3 mm with the exposure time of 500 ms per projection, and the number of projections are1000. Nrecon software was used to reconstruct the 3D structure, and CTVox software was used to visualize the reconstructed sample in 3D. CTAN software was used for analyzing the void datas. The CT scan produces 2D cross-sectional and 3D reconstructions images, providing detailed visualization of internal geometry and porosity. Key parameters such as porosity (%), channel diameter, wall thickness, and structural integrity were analysed. A consistent ROI-(Region of Interest) cylinder of 3.5 mm diameter × 12 mm height was extracted from the central region of each sample to avoid edge artifacts and surface irregularities due to boundary effects. This standardization ensured comparable data between the 5-channel and 6-channel structures. Measurements were performed in triplicate, and standard deviation/error was calculated for porosity and pore size distribution to ensure repeatability to assess the effect of channel number and distribution on material performance. The results provide valuable insights into the structural integrity of the lotus root structures.

2.3.3. *Antibacterial activity*

Following ISO 5833:2002 [23], the antibacterial activity of the samples were tested using the nutritious well diffusion method. strains of the bacteria S aureus and E coli were utilized in the antibacterial test. The bacteria were injected into the nutrient agar plates, which was maintained in an aseptic environment, using a glass L-rod and 100 µl of growing culture. Sterilized lotus root structures (solid, five-channel, and six-channel) were gently placed onto the surface of inoculated agar plates, ensuring proper contact. A squire (10 mm) and a thin film coated with a chemical (antimicrobial agent), were applied after each plate had been incubated for 48 h at 37 °C. The zone of inhibition was measured and reported in millimetres (mm) after the incubation period. The concentration at which bacteria are unable to grow is known as the minimum inhibitory concentration (MIC). agar.

2.3.4. Live/dead cell staining

Osteoblast-like cells (MC3T3-E1) were used for the study, with a seeding density of 1×10^4 cells/cm^2 and cultured for 1, 7, and 14 days. Cell viability was assessed based on fluorescence intensity thresholds, where green fluorescence values greater than 60 intensity units indicated viable cells, and red fluorescence values above 40 intensity units represented dead cells. To visualize live and dead viability was assessed using the Calcein-AM and Ethidium Homodimer-1 (EthD-1) staining kit. On days 1 and 7, the lotus root structures were rinsed gently with PBS to remove non-adherent cells and incubated with the staining solution (2 μM Calcein-AM and 4 μM EthD-1 in PBS) for 30 min at 37 °C. After staining, the structures were visualized using a fluorescence microscope (excitation/emission: 488 nm for Calcein-AM and 528 nm for EthD-1). Live cells stained green (Calcein-AM), while dead cells stained red (EthD-1). Images were captured, and the live/dead cell ratio was quantified using ImageJ software. Each experimental group included three biological replicates and three technical replicates to maintain statistical reliability.

2.3.5. In vitro hemocompatibility- hemolysis assay

The study used lotus root structures for a hemolysis test, following ASTM F756-17 standards [24].

The disc-shaped samples were made 12 mm and (diagonal length: 350 mm), and wall thickness of 1.0 mm, such that the surface area of the samples is sufficiently exposed to blood in the contact assays, with 3 cm^2/mL for negative controls (PBS) and 6 cm^2/mL for positive controls (distilled water).

Blood was collected and diluted with PBS in a 1:9 ratio, kept at 4 °C for minimal degradation of red blood cells. Samples were prepared for testing in three different structures (solid, 5-channel, and 6-channel) and rinsed thoroughly. Three replicate samples were placed in separate tubes containing 5 mL of diluted blood (10 % blood concentration) and incubated at 37 °C for 1 h. The blood samples were centrifuged at 1500 rpm for 5 min to separate the supernatant, which was then collected to assess hemolysis extent. The hemolysis percentage was determined by measuring the absorbance of the supernatant at 540 nm using a UV–visible spectrophotometer.

$$\text{Hemolytic } (\%) = \frac{\text{OD (sample)- OD (negative control)}}{\text{OD (positive control) - OD (negative control)}} \times 100 \quad (1)$$

According to ISO 10993-4 1999 materials are considered hemocompatible if the hemolysis percentage is less than 5 %. Values above this threshold indicate potential homolytic activity [25].

2.3.6. Compression test

The compression test was performed to evaluate the mechanical performance of the fabricated lotus root structures. Cylindrical specimens with a diameter of 10 mm and a height of 20 mm were prepared from each design (solid, 5-channel, and 6-channel). The compressive test was conducted using a universal testing machine (Model: INSTRON 8801) in accordance with followed ISO 5833-2002 specifications with a compression rate of 1 mm/min Before testing, all specimens were conditioned in a simulated body fluid (SBF) at 37 °C for 7 days to simulate in vitro conditions [26].

2.4. Statistical analysis

The JMP Pro statistical analysis tool was employed to execute the statistical investigation. One-way analysis of variance (ANOVA) was employed to identify significant differences in the Physicochemical, Mechanical, and Bioactive Characteristics of the varying channel configurations (solid, 5-channel, and 6-channel) under a confidence level of 95 %. This investigation presents in four distinct the value, all date were expressed as means standard ± deviation (SD). A p-value <0.05 was considered statistically significant.

3. Result and discussion

3.1. Scanning electron microscopy (SEM) analysis

The surface morphology of 25%AKT/PMMA/25%ZrO_2 composites was analysed using SEM to evaluate the effect of different lotus root-inspired channel designs fabricated through bio plotter additive manufacturing. The tested structures included 5-channel and 6-channel. SEM images of the 5-channel structure are demonstrated in Fig. 5. The successful incorporation of designed channels although minor surface irregularities were observed, likely due to printing layer boundaries and differences in material deposition rates [27]. The walls of the channels maintained consistent material blending, and the reinforcement particles were well-distributed. Localized porosity clusters will influence mechanical properties and enhance cell attachment. However, some areas exhibited localized porosity clusters, potentially due to material flow challenges [28]. These clusters could influence the mechanical properties but might also challenges in cell proliferation. The SEM images provided insights into the distribution of composite materials, pore connectivity, and overall structural integrity. The SEM analysis of the 6-channel structure is shown in Fig. 6, similar trends to the 5-channel structure but with a more pronounced porosity near the channel boundaries. The increased number of channels introduced slightly uniform interfacial gaps between layers. The channel walls exhibited a uniform material distribution. The particulate distribution of ZrO_2 and AKT remained consistent along the walls, with no significant agglomeration or segregation. However, compared to the 5-channel structure, the porosity around the channel boundaries was slightly increased. This enhanced porosity could facilitate fluid transport and osseointegration, aligning with the intended orthopaedic application. Interfacial gaps between printed layers were visible at higher magnifications, which may impact the mechanical stability overall surface morphology suggests that the 6-channel design offers a promising balance between porosity and mechanical strength, and suitable for applications requiring higher bioactivity and fluid interaction.

The SEM analysis of the two channel highlights the trade-offs between structural integrity and porosity introduced by the channel designs. The presence of minor interfacial gaps in the 5-channel and 6-channel structures additionally refer to the increased porosity near the channels might provide pathways for nutrient transport, improving the scaffold's suitability for orthopaedic tissue engineering. SEM analysis confirmed the feasibility of fabricating lotus root-inspired channel designs using Bioplotter AM for 25%AKT/PMMA/25%ZrO_2 composites. Each design exhibited distinct advantages the 5-channel structure offered excellent compactness and potential mechanical high strength, while the 6-channel structures demonstrated enhanced porosity and surface morphology conducive to biological interactions.

The EDX analyses shown in Fig. 7 (a)5channel, (b)6channel indicate higher concentrations of Akermanite (AKT) resulted in more prominent Si and Mg peaks, while the Zr became more distinct, suggesting improved dispersion and incorporation of ZrO_2 within the PMMA matrix. The elemental distribution and strong interfacial bonding between PMMA and the incorporated phases. which correlates with enhanced superior bone-bonding characteristics.

3.2. 3D micro-Computed Tomography (Micro-CT) analysis

Fig. 8 shows the 5 channels, (5C) and 6 channels (6C) Micro-CT images, the micro-CT analysis on the 5-channel design presented a significant improvement in porosity. The Micro-CT images showed a more interconnected network of channels, enhancing the overall porosity and surface area available for osteointegration [29]. The porosity was found to be within the ideal range for bone tissue scaffolds, which typically require porosity values of around 53 ± 1 % for optimal cell infiltration

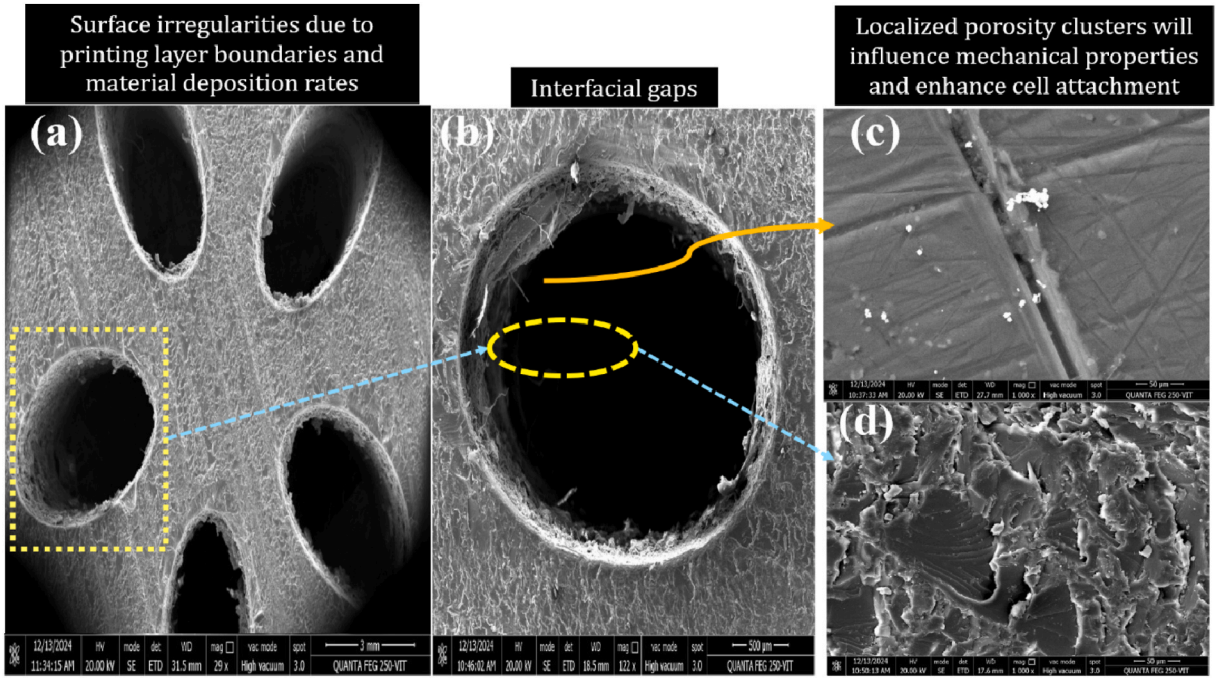

Fig. 5. Surface morphology study of 5-channel structures (FESEM micrographs). **(a)** 5channel, **(b)** single channel of 5 channels structure **(c,d)** high magnification of single channel of 5 channels structure.

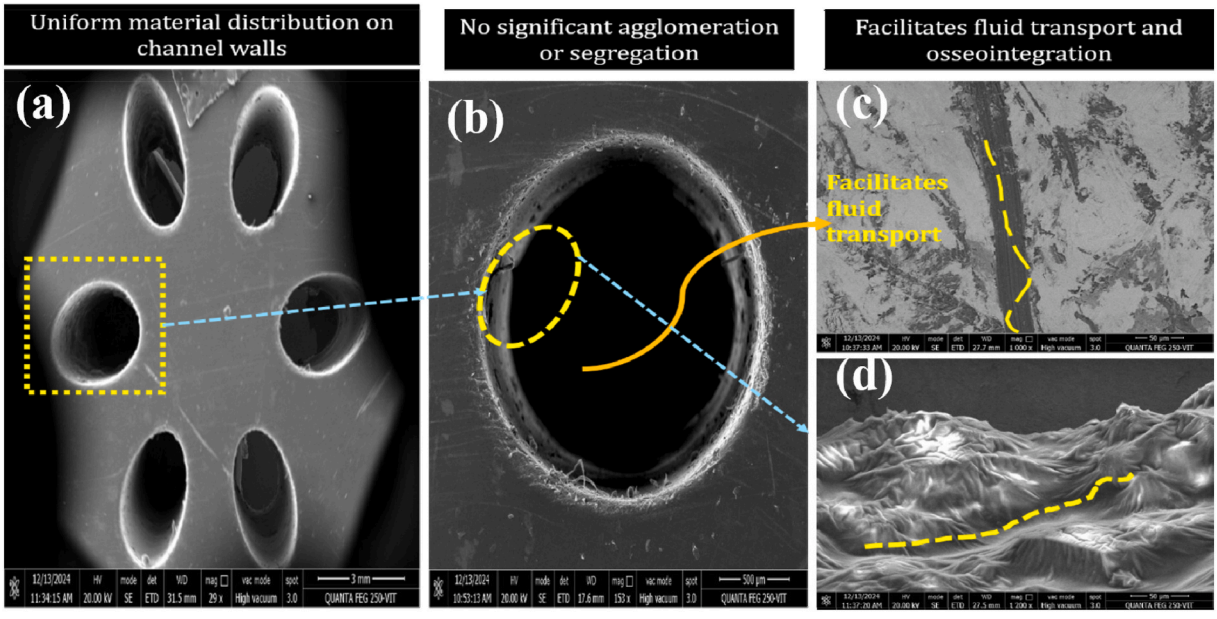

Fig. 6. Surface morphology study of 6-channel structures (FESEM micrographs) -**(a)** 6channel, **(b)** single channel of 6 channels structure **(c, d)** high magnification of single channel of 6 channels structure.

and vascularization. The 6-channel configuration offered a balance between structural integrity and biological functionality, and limit the potential for promoting bone in-growth or fluid diffusion, which are important considerations for implant integration and long-term success.

The 6-channel exhibited an even greater porosity 67 ± 3 % than the 5-channel structure, with a well-developed network of interconnecting channels. Micro-CT imaging revealed enhanced porosity and more efficient inter-channel connections, which could facilitate better vascularization and nutrient exchange. However, the increased number of channels also slightly reduced the material's overall mechanical strength compared to the 5-channel structure. This configuration might be better suited for applications where a higher degree of porosity is required [30], such as in scenarios where rapid tissue ingrowth or higher surface area for biological interactions is desired. The 6-channel design could enhance the healing process in orthopaedic applications, as the interconnected channels promote the migration of osteoblasts and blood vessels.

The Micro-CT analysis provided valuable insights into the impact of channel design on the structure and porosity of the composite materials. The 5 C structures, while offering the highest mechanical strength, may not support fluid exchange in tissue regeneration as effectively as the channel design. On the other hand, in comparison with 6-channel

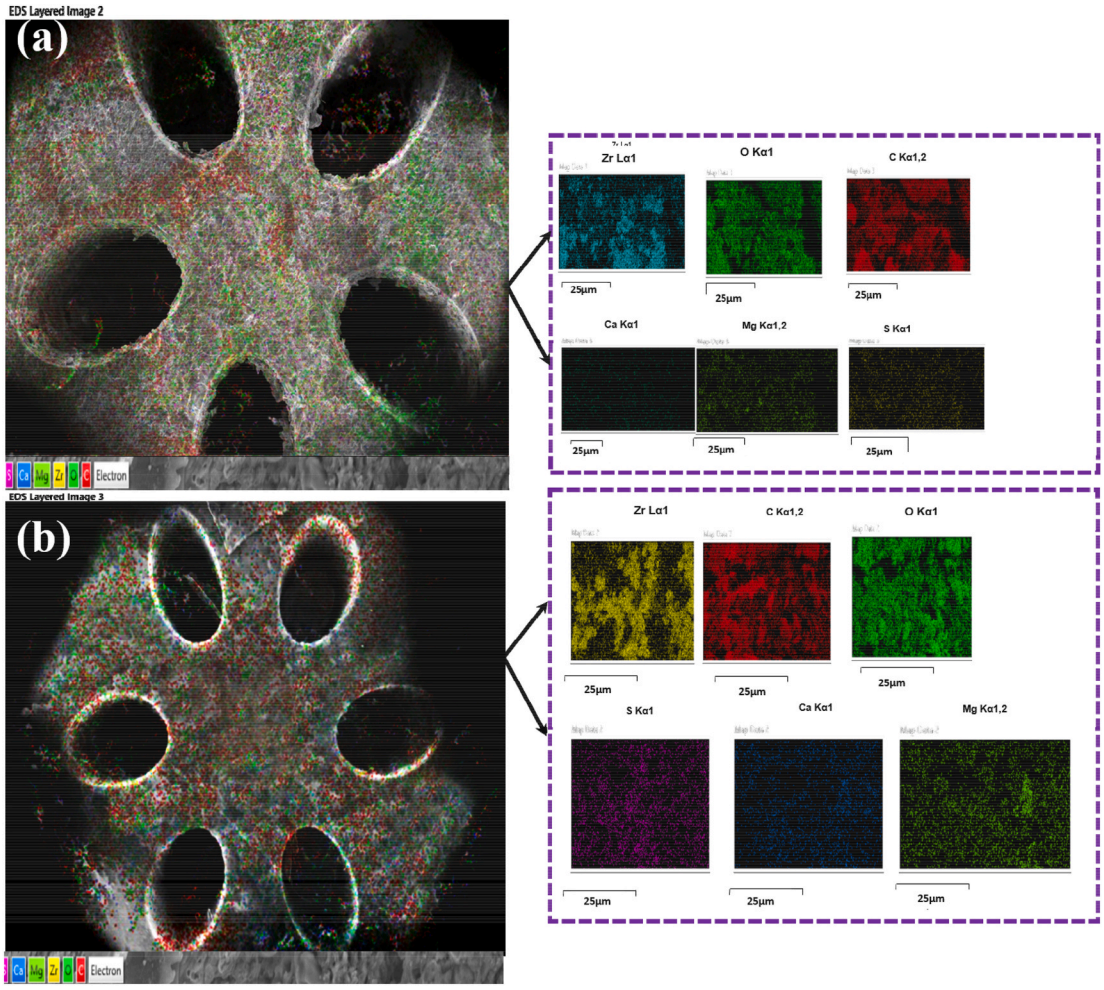

Fig. 7. EDS examination and elemental mapping on lotus root structure **(a)** 5Channel, **(b)** 6 Channel.

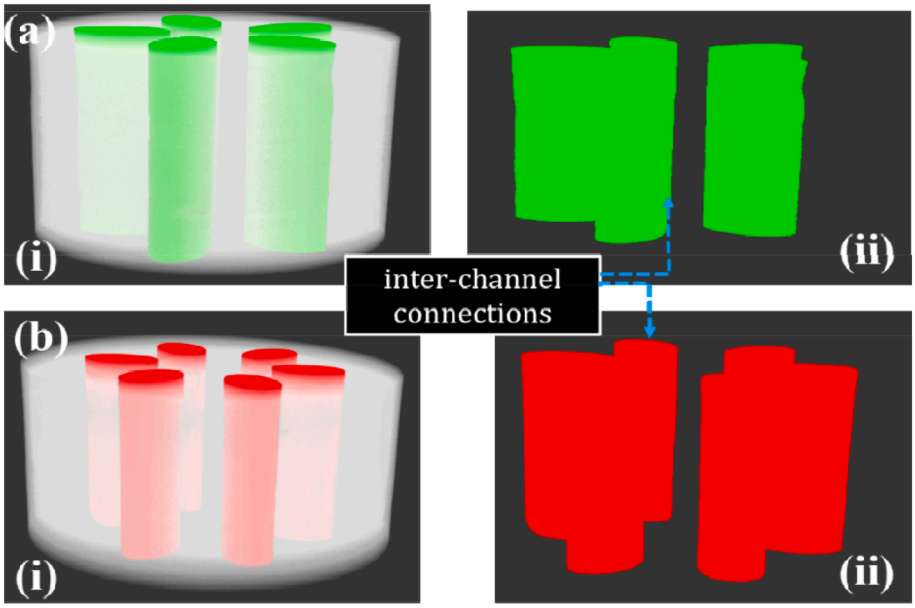

Fig. 8. Micro-CT images **(a)** 5-channel, **(b)** 6-channel **(i)** 3D lotus root structure scaffolds **(ii)** inter-channel connection.

structures, although slightly reducing the mechanical integrity, improves the composite's biological functionality, by supporting tissue ingrowth and enabling efficient nutrient flow. The porosity analysis for the 6 Channel structure exhibited a statistically significant ($p < 0.05$) when compared over the other groups of channel structure.

3.3. In vitro antibacterial activity

Fig. 9 exhibits the antibacterial effect of different channel structure against Staphylococcus (*S. aureus*), and *Escherichia coli* (and *E. coli* aureus). The solid structure of the composite demonstrated moderate inhibition of both *S. aureus* and *E. coli* growth. The zone of inhibition for *S. aureus* was approximately 6 ± 1 mm, while for *E. coli*, it was around 5 ± 0.8 mm. This suggests some degree of antibacterial activity, likely due to the inherent properties of the ZrO_2 and AKT components.

The 5-channel structure exhibited a more significant antibacterial effect compared to the solid structure. The zone of inhibition for *S. aureus* increased to 14 ± 3 mm, while for *E. coli*, it was approximately 12±1 mm. The increased surface area provided by the channels enhanced the exposure of the composite to the bacterial colonies, promoting greater antibacterial action. The interconnected channels likely facilitated better diffusion of antimicrobial ions and allowed for more effective bacterial inhibition at the material surface. This configuration could enhance the diffusion of antimicrobial agents, facilitating better interaction with the bacterial cells. The 6-channel lotus root structure showed the highest antibacterial activity, with zones of inhibition measuring 21 ± 0.6 mm for *S. aureus* and 16 ± 1.2 mm for *E. coli* as shown in Figs. 9 and 10.

The higher porosity and increased surface area, coupled with the larger number of channels, further improved the material's ability to release antibacterial ions and inhibit bacterial growth. Additionally, the 6-channel design increasing exposure of the composite to the surrounding medium. The enhanced surface area facilitates greater release of Ca^{2+} and Mg^{2+} ions from Akermanite, which are known to disrupt bacterial cell walls and inhibit bacterial proliferation [31], enhancing the overall antimicrobial effect and facilitate the release of ions with bactericidal properties, further contributing to bacterial growth inhibition. ZrO_2 provide additional antibacterial activity by generating reactive oxygen species (ROS) at the material surface under physiological conditions, further inhibiting bacterial colonization [32]. Results demonstrate that promising antibacterial activity, particularly in 6-channel lotus root structures, enhance medium penetration, leading to more efficient ion exchange and improved antibacterial performance compared to solid constructs. For the antibacterial ability of 6 Channel structure exhibited a statistically significant ($p < 0.05$) when compared over the other groups of channel structure.

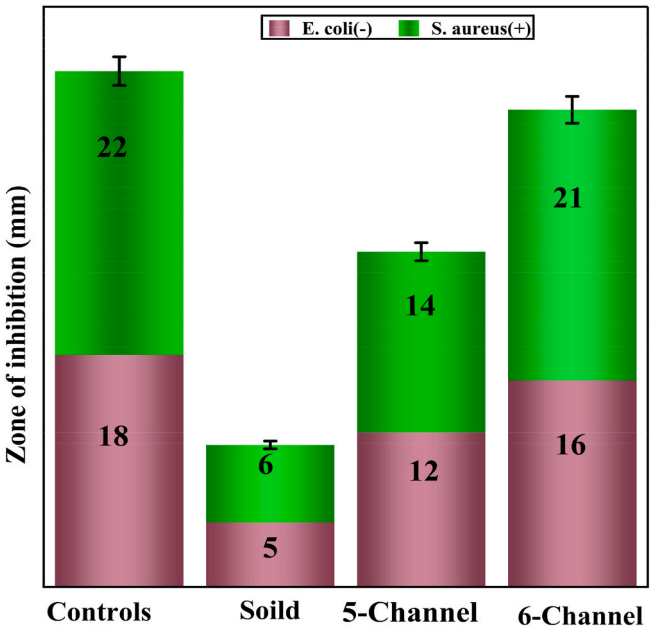

Fig. 10. Bacterial inhibition size (mm).

3.4. The bioactivity study - SBF preparation, and measuring the pH

Bone cement being subjected to in vitro bioactivity investigation. A change in the pH level of the SBF mixture was detected after immersing over time (1–14days) for solid, 5-channel, and 6-channel structure as shown in Fig. 11. The results revealed a gradual increase in pH during the initial immersion period, indicating the release of Ca^{2+}, Mg^{2+}, and Si^{4+} ions from the AKT phase, which promoted apatite nucleation. The pH increased 2 days for the 6-channel structure, while the 5-channel and solid structures showed slightly lower increments. This variation reflects the enhanced ion exchange kinetics facilitated by the increased surface area and fluid permeability of the porous structures. After 5 days, the pH values stabilized around 7.41 ± 0.03 for 5 and 6 channel structures, suggesting equilibrium between ion release and apatite deposition.

Overall, the 6-channel lotus stem structure exhibited the highest pH variation and bioactive response, attributed to its interconnected pore network, which enhanced fluid interaction and ion diffusion. These findings confirm that the additive-manufactured lotus stem-inspired structure, particularly the 6-channel design, supports pH environment is unfavourable for bacterial growth and contributes to the observed

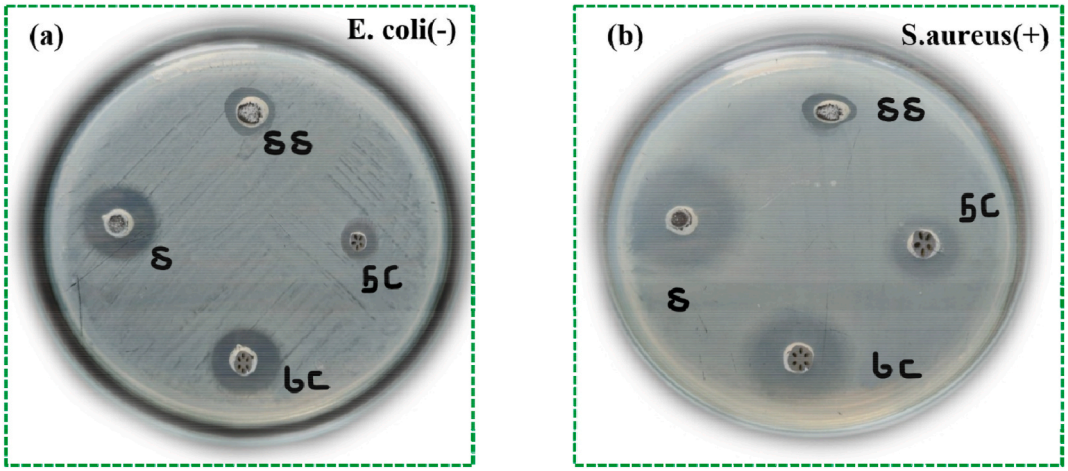

Fig. 9. (a) *E. coli* (−) and **(b)** *S. aureus* (+) - Images of the sample's inhibition zones after 48 h.

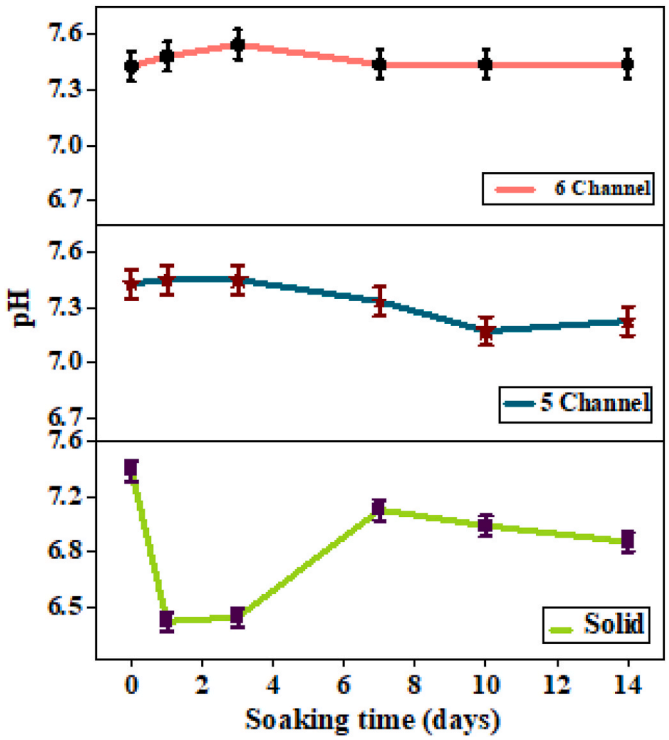

Fig. 11. pH value obtained for the solid structure, 5-channel, and 6-channel lotus root structures with different soaking times in days.

antibacterial effect.

3.5. Assessment of live/dead cell viability

The Live/Dead Cell Viability Analysis of composite structures fabricated using bioplotter additive manufacturing was evaluated on Day 1 and Day 7 for three different designs: solid structure, 5-channel, and 6-channel lotus root structures. The live/dead assay was used to qualitatively assess cell viability and spatial distribution on the fabricated lotus root structures are presented in Figs. 12 and 13.

Day 1 showed the live/dead staining revealed predominantly live cells (green fluorescence) across all structures, with minor dead cells (red fluorescence) detected. In the solid structure exhibited less uniform cell distribution, with fewer dead cells observed in the core regions, due to limited nutrient and oxygen diffusion with moderate proportion of live cells (60 ± 7 %), The 5-channel structure had 85 ± 5.4 % live cells, with homogeneously distributed fluorescence across the scaffold. The 6-channel structure showed a uniform distribution of live cells along the channel walls and within the pores, indicating effective cell attachment, this structure achieved >95 % (96 ± 06 %) live cells, with vibrant fluorescence in both peripheral and core regions, confirming enhanced cellular viability due to effective channel design.

On Day 7, the solid structure exhibited a slight decrease in live cell viability (55 ± 2.6 %) near the core regions with moderate dead (red) cells, potentially due to diffusion limitations peripheral regions however maintained 60 % live cells with few dead (red) cells in region.

The 5-channel structure retained (79 ± 1.4 %) live cells overall, with a significant presence of viable cells across the scaffold with slightly lower cell density compared to the 6-channel design with few dead (red) cells in peripheral regions compare with solid structure. The 6-channel structure maintained high cell viability >95 %, (91 ± 0.7 %) with dense live cell coverage observed throughout the scaffold, including the internal channels, indicating sustained cellular health and proliferation throughout the scaffold. Cell viability analysis exhibited a statistically significant ($p < 0.05$) when compared over the other groups of channel structure.

3.6. In vitro hemolytic assay

The hemolysis test was conducted to assess the biocompatibility of composites in different structures. Table 1, it is evident that the hemolytic percentage of solid structure, 5-channel, and 6-channel exhibits minimal red blood cell damage, confirming its biocompatibility for orthopaedic applications. The solid composite structure exhibited a hemolysis percentage of 4.89 ± 2 %, which is within the acceptable range for biomaterials as per ISO 10993-4 standards (less than 5 %). The absence of any significant damage to red blood cells suggests the material's suitability for implantation [33].

Fig. 14 shows that the 5-channel lotus root structure demonstrated a slightly lower hemolysis percentage of 4.61 ± 1.6 %. The presence of channels did not lead to any increased cell lysis, suggesting that the porous nature of the structure does not negatively affect the material's interaction with blood. The 6-channel lotus root structure exhibited the lowest hemolysis percentage at 3.13 ± 0.8 %. This slight reduction in hemolysis could be attributed to the increased surface area and enhanced fluid dynamics provided by the additional channels, which may help in distributing the blood flow more evenly, thus reducing potential cell damage. The haemolytic effect for the 6-channel structure exhibited a statistically significant ($p < 0.05$) when compared over the other groups of channel structure.

The 5-channel and 6-channel designs showed slightly reduced hemolysis compared to the solid structure, possibly due to increased surface area and better blood flow integration within porous channels. This could reduce pressure points that could cause red blood cell rupture [34]. The microstructural design also plays a role in improving the composite's overall performance, potentially enhancing tissue integration and function in orthopaedic applications. The materials meet the necessary standards for safe use in orthopaedic implants.

3.7. Compression test

The different channel lotus root structure designed to mimic the mechanical behavior of cortical bone for orthopaedic applications, the result is presented in Figs. 15 and 16. The solid structure exhibited the highest compressive strength (145.6 ± 2 MPa), Young's modulus (6.5 ± 1.2 GPa) and strain rate (0.0224 (2.24 %)) among the tested designs. This is attributed to its fully dense geometry, which maximizes load-bearing capacity and minimizes stress concentration points. The performance of the solid structure is well-suited for cortical bone applications, as its properties align closely with the mechanical requirements of natural bone. The absence of channels results in enhanced load-bearing capacity, but it compromises the potential for vascularization and nutrient transport, critical for long-term osseointegration and bone remodelling. The 5-channel structure showed a moderate reduction in compressive strength) and Young's modulus compared to the solid structure.

The introduction of 5-channels resulted in a moderate reduction in compressive strength (132.8 ± 4 MPa), Young's modulus (5.9 ± 0.4 GPa) and strain rate (0.0224 (2.24 %)). This design provided a balance between mechanical strength and porosity, which is beneficial for enhancing bio integration and vascularization.

The arrangement of 5-channels provides a compromise between mechanical support and biological functionality, making it suitable for applications requiring moderate porosity without significant loss in strength. The 6-channel structure showed the lowest compressive strength (120.5 ± 6 MPa), Young's modulus (5.4 GPa), and the strain rate 0.0223 (2.23 %) due to the increased porosity and reduced material volume. While this structure sacrifices some mechanical properties, it offers the highest potential for nutrient and fluid transport, which is advantageous for cellular activity and osseointegration in orthopaedic applications. However, care must be taken to ensure the mechanical

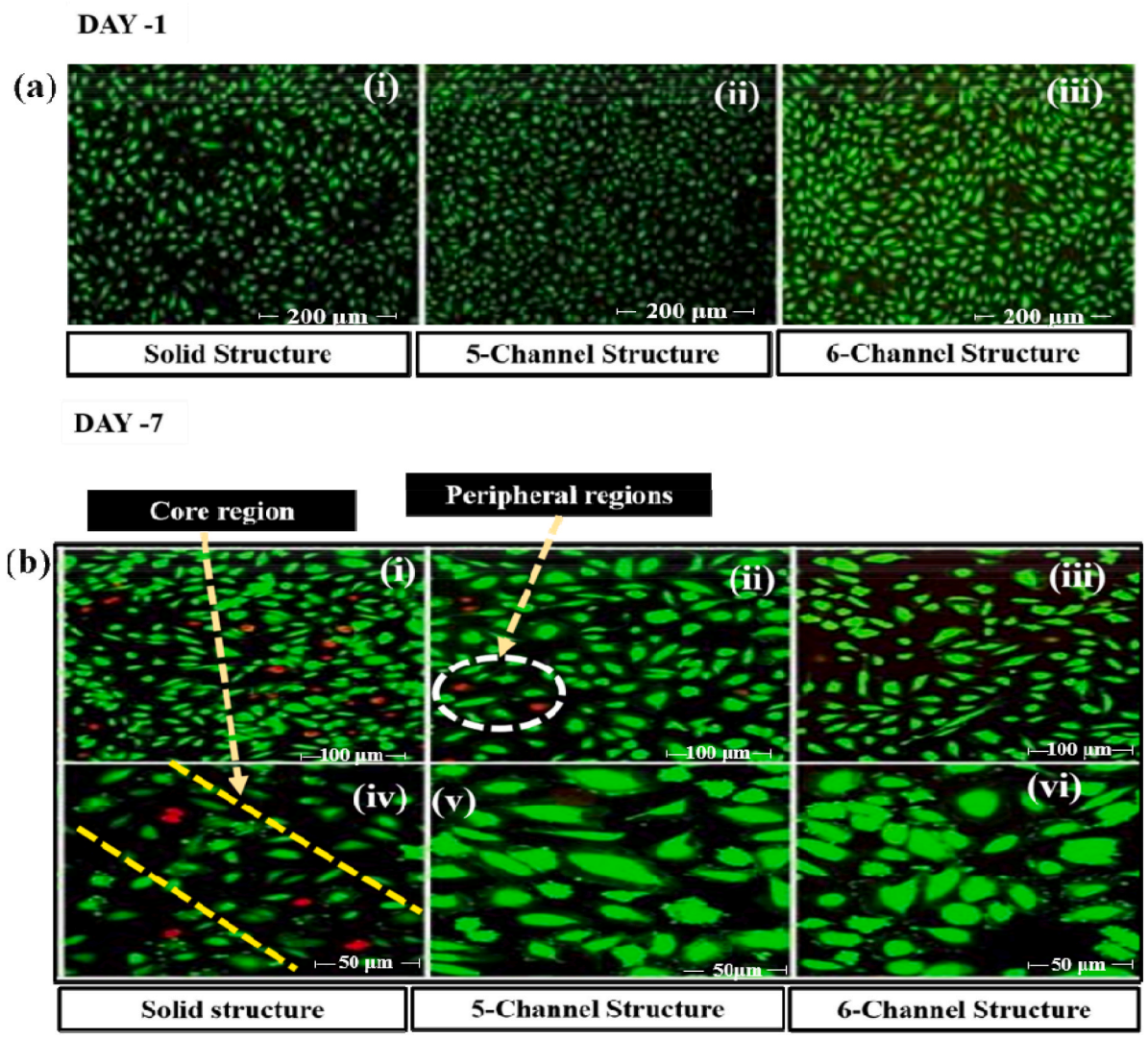

Fig. 12. Live/Dead cell viability assay (green) and non-viable (red) cells on the sample surface **(a)** Low magnification-(i-iii-(scale bar = 200 µm)) **(b)** High magnifications-(i-iii-(scale bar = 100 µm)), (iv-vi-(scale bar = 50 µm)).

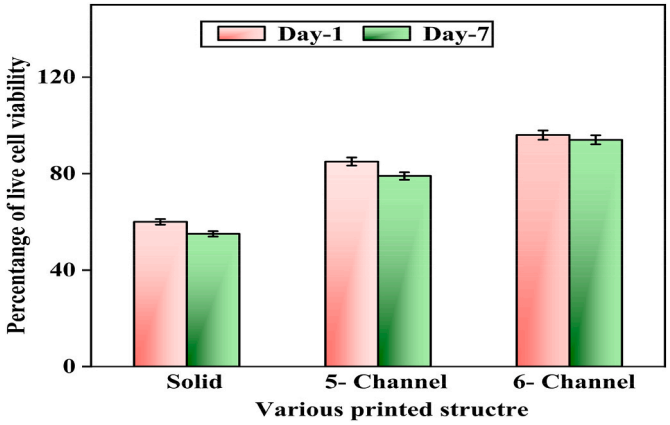

Fig. 13. Live/Dead cell viability % for the variant structure-(Solid,5-channel,6-channel).

Table 1
Hemolytic percentage of different structure.

Sample	Optical Density (OD) value	Hemolytic (%)
Positive control (+) (Distilled Water)	2.27	5
Negative control (−) (PBS)	0.45	2
Solid structure	0.539	4.89
5-Channel structure	0.534	4.61
6-Channel structure	0.48	3.13

properties remain within the acceptable range for cortical bone substitution [35,35] The compressive strengths, young's modulus and strain rate of exhibited a statistically significant ($p < 0.05$). The results are summarized in Table 2.

3.8. Statistical analysis

The JMP Pro statistical analysis tool was used to perform the statistical analysis. In order to determine whether or not there were significant differences in the Physicochemical, Mechanical, and Bioactive Properties of the 25%KT/PMMA/25%ZrO_2 Versus Properties, a one-way

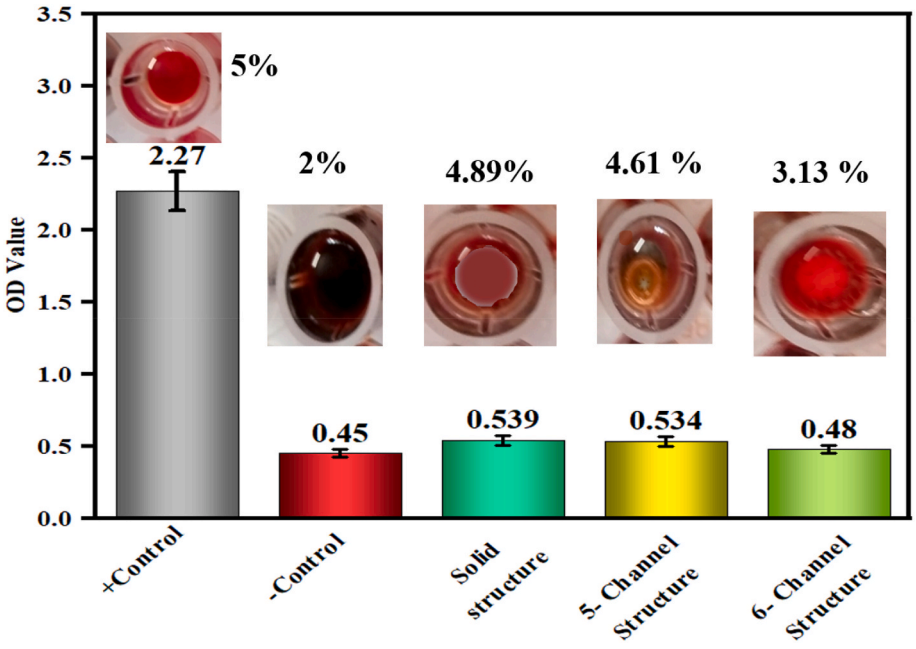

Fig. 14. Hemolytic activity.

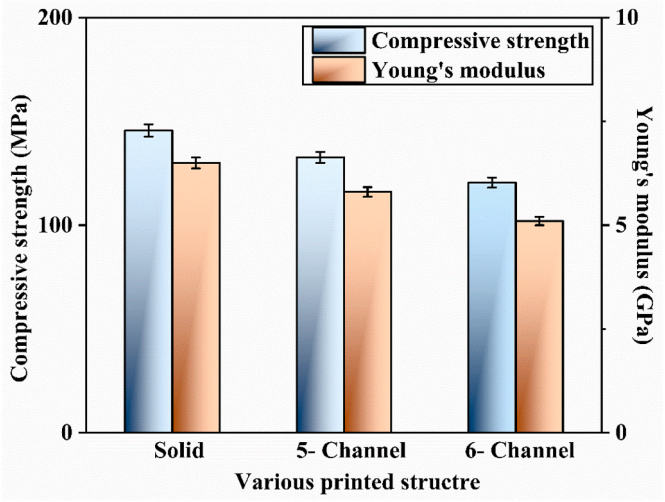

Fig. 15. Mechanical characteristics of various printed structure.

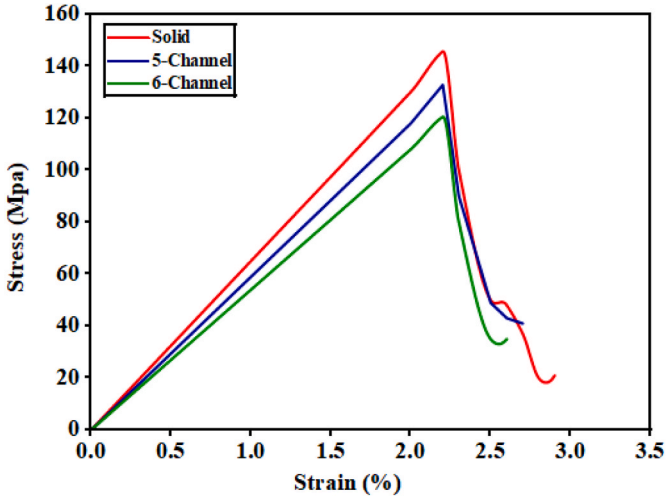

Fig. 16. Stress–strain curves of different channel configurations (solid, 5-channel, and 6-channel).

analysis of variance (ANOVA) was performed with a confidence level of 95 %. This investigation presents in varying channel configurations (solid, 5-channel, and 6-channel). Table 3 provides comprehensive information on the relevant parameters, including the sum of squares, mean sum of squares, degree of freedom, F-value, and P-value for mechanical and physical properties.

The 'F' actual value surpasses the 'F' essential value, suggesting that the results from each group are statistically different by chance. The variation is significant at the 95 % confidence level, demonstrated by a 'P' value less than 0.05. There are statistically significant differences in the material's properties between the average values of the different groups.

4. Conclusions

The investigation of 25%AKT/PMMA/25% ZrO_2 composites fabricated using a bio plotter additive manufacturing process demonstrates the potential of these materials for orthopaedic applications. Three lotus root-inspired structures such as solid, 5-channel, and 6-channel structures were developed and analysed to evaluate their physical, mechanical, and biological properties.

- The results revealed that the inclusion of AKT and ZrO_2 significantly enhanced the composite's bioactivity and mechanical performance.
- In the current study, the 25%AKT/PMMA/25% ZrO_2 composites were studied in terms of lotus root-inspired structures (solid, 5-channel and 6-channel) made in a bio plotter additive manufacturing (AM) procedure to determine the suitability of the composite material in orthopaedic applications. The results indicate how essential structural design is when it comes to balancing between mechanical integrity and biological functionality.
- The compressive strength was shown to be superior in all the structures, with the solid design, though with high mechanical performance, showing low osteoconductivity, attributable to the lack of sufficient interconnected porosity.

Table 2
The summarized results of biomechanical properties for the 3D-printed lotus root structure.

Sample	Compressive strength (MPa)	Young's modulus (GPa)	Strain rate	porosity. (%)	Hemolytic (%)	Inhibition zones –S aureus (mm)	Inhibition zones –E. coli (mm)	cell viability (%) (Day-1)	cell viability (%) (Day-7)
Solid structure	145.6 ± 2	6.5 ± 1.2	0.0224 (2.24 %)	–	4.89 ± 2	6 ± 1	5 ± 0.8	60 ± 7	55 ± 6
5-Channel structure	132.8 ± 4	5.9 ± 0.4	0.0225 (2.25 %)	53 ± 1	4.61 ± 1.6	14 ± 3	12 ± 1	85 ± 5.4	79 ± 1.4
6-Channel structure	120.5 ± 6	5.4 ± 0.8	0.0223 (2.23 %)	67 ± 3	3.13 ± 0.8	21 ± 0.6	16 ± 1.2	96 ± 2	91 ± 0.7
Standard**	100–230	5–7	0.014–0.046 (1.4–4.6 %)	>55	<5	22	18	90–100	90–100

Table 3
Statistical analysis of varying channel configurations (solid, 5-channel, and 6-channel).

Source	DOF	Sum of Squares	Mean square	'F' Ratio	Prob > F
Porosity (%)	3	1196.7412	398.914	386.8817	**<.0001***
	12	12.3732	1.031		
	15	1209.1144			
Inhibition zones -S aureus (mm)	3	121.32688	40.4423	177.9313	**<.0001***
	12	2.72750	0.2273		
	15	124.05438			
Inhibition zones –E. coli (mm)	3	40.671875	13.5573	74.3714	**<.0001***
	12	2.187500	0.1823		
	15	42.859375			
Cell viability (%)	3	4436.0000	1478.67	887.2000	**<.0001***
	12	20.0000	1.67		
	15	4456.0000			
pH	3	0.11261875	30.037540	1.7324	**<.0005***
	12	0.26002500	0.21669		
	15	0.37264375			
Hemolysis	3	67.162225	18.4732	2.1452	**<.0005***
	12	4.3650	0.48321		
	15	71.0614			
Compressive strength (MPa)	3	74.221625	24.7405	4230.299	**<.0001***
	12	6.863750	0.5720		
	15	81.085375			
Youngs modulus (Mpa)	3	163659.69	54553.2	1573.228	**<.0001***
	12	154.75	12.9		
	15	163814.44			

- Micro-CT analysis ensured that the 5-channel and 6-channel structures provided effective interconnectivity that favored enhanced porosity and scaffold integration-fundamental parameters to ensure the process of osseointegration and transport of nutrients.
- The most favourable result was demonstrated in the 6-channel structure which had high cell viability (>90 %) and dense live cell coverage on both the exterior and interior areas of the scaffold. This performance was a best balance of compressive strength and biological functionality. Whereas the compressive strength of cortical bone generally within the 100–200 Mpa range and Youngs modulus of 5–7 Gpa, the 6-channel design allowed sufficient mechanical stability and higher porosity of the bone tissue to grow in.
- These findings highlight the fact that the 6-channel lotus root-like structure has the least trade-off between structural stability and bio functionality and is, therefore, potentially useful in orthopaedics where load-bearing capacity is required together with biological integration.
- Overall, this research establishes the possibilities of bioplotter AM in order to create complex biomaterial scaffolds with uniform characteristics. With this method, they are able to create sophisticated bone substitutes with specific mechanical and biological properties as this technique allows the design of multi-channel structure. demonstrated promising to cortical bone. Future applications of these composites may extend beyond standard orthopedic bone cements to include maxillofacial and cranial implants, broadening the clinical impact and potential of this work.

Authors' contributions

Girija M: writing - review and editing, writing- original draft, methodology, investigation, visualization, conceptualization, formal analysis, and data curation.

Sampath Kumar T: investigation, formal analysis, data curation, reviewing- original draft and supervision.

Sumsun Naher: Data curation, reviewing- original draft and supervision.

Data availability statement

All data generated or analysed during this study are included in this published article.

Disclosure statement

No potential conflict of interest was reported by the author(s)

Declaration of competing interest

The authors declare that they have no known competing financial interests or personal relationships that could have appeared to influence the work reported in this paper.

Acknowledgments

The authors thank VIT University for providing the facilities to carry out the research and School of Mechanical Engineering, VIT University Vellore and Department of Science and Technology. New Delhi, India for providing financial support to acquire 'Micro CT Scan Facility' through 'Promotion of University Research and Scientific Excellence (PURSE)' under Grant No. SR/PURSE/2020/34 (TPN 56960) and carry out the necessary facilities for this research work.

References

[1] Alam MI, Kashyap S, Balaji PG, Yadav AK, Flora SJS. 3D-Printed medical implants: recent trends and challenges. Biomedical Materials and Devices 2025;3:750–70. https://doi.org/10.1007/s44174-024-00221-0.
[2] Guzzi EA, Tibbitt MW. Additive manufacturing of precision biomaterials. Adv Mater 2020;32. https://doi.org/10.1002/adma.201901994.
[3] Agarwal R, Gupta V, Singh J. Additive manufacturing-based design approaches and challenges for orthopaedic bone screws: a state-of-the-art review. J Braz Soc Mech Sci Eng 2022;44:1–25. https://doi.org/10.1007/s40430-021-03331-8.
[4] Sprio S, Panseri S, Montesi M, Dapporto M, Ruffini A, Dozio SM, et al. Hierarchical porosity inherited by natural sources affects the mechanical and biological behaviour of bone scaffolds. J Eur Ceram Soc 2020;40:1717–27. https://doi.org/10.1016/j.jeurceramsoc.2019.11.015.
[5] Zhao W, Huang Z, Liu L, Wang W, Leng J, Liu Y. Porous bone tissue scaffold concept based on shape memory PLA/Fe3O4. Compos Sci Technol 2021;203:108563. https://doi.org/10.1016/j.compscitech.2020.108563.
[6] Cheng KC, Theato P, Hsu SH. 3D-bioprintable endothelial cell-laden sacrificial ink for fabrication of microvessel networks. Biofabrication 2023;15. https://doi.org/10.1088/1758-5090/acfac1.
[7] Rezwan K, Chen QZ, Blaker JJ, Boccaccini AR. Biodegradable and bioactive porous polymer/inorganic composite scaffolds for bone tissue engineering. Biomaterials 2006;27:3413–31. https://doi.org/10.1016/j.biomaterials.2006.01.039.
[8] Huang K, Huang J, Zhao J, Gu Z, Wu J. Natural lotus root-based scaffolds for bone regeneration. Chin Chem Lett 2022;33:1941–5. https://doi.org/10.1016/j.cclet.2021.10.073.
[9] Feng C, Zhang W, Deng C, Li G, Chang J, Zhang Z, et al. 3D printing of Lotus root-like biomimetic materials for cell delivery and tissue regeneration. Adv Sci 2017;4. https://doi.org/10.1002/advs.201700401.
[10] Veeman D, Sai MS, Sureshkumar P, Jagadeesha T, Natrayan L, Ravichandran M, et al. Additive manufacturing of biopolymers for tissue engineering and regenerative medicine: an overview, potential applications, advancements, and trends. Int J Polym Sci 2021;2021. https://doi.org/10.1155/2021/4907027.
[11] Mohammadi Zerankeshi M, Mofakhami S, Salahinejad E. 3D porous HA/TCP composite scaffolds for bone tissue engineering. Ceram Int 2022;48:22647–63. https://doi.org/10.1016/j.ceramint.2022.05.103.
[12] Zafar MS. Prosthodontic applications of polymethyl methacrylate (PMMA): an update. Polymers 2020;12:1–35. https://doi.org/10.3390/polym12102299.
[13] Edo GI, Ndudi W, Ali ABM, Yousif E, Zainulabdeen K, Onyibe PN, et al. An updated review on the modifications, recycling, polymerization, and applications of polymethyl methacrylate (PMMA). J Mater Sci 2024;59:20496–539. https://doi.org/10.1007/s10853-024-10402-3.
[14] Girija M, Sampath Kumar T. Characterization of akermanite (AKT) and zirconia-infused PMMA bone cement composite with superior physicochemical, mechanical, and bioactive properties for enhanced orthopaedic performance. Compos Interfaces 2025;32:817–41. https://doi.org/10.1080/09276440.2024.2442169.
[15] Ahmadipour M, Mohammadi H, Pang AL, Arjmand M, Ayode Otitoju T, Okoye P U, et al. A review: silicate ceramic-polymer composite scaffold for bone tissue engineering. International Journal of Polymeric Materials and Polymeric Biomaterials 2022;71:180–95. https://doi.org/10.1080/00914037.2020.1817018.
[16] Ozbolat IT, Moncal KK, Gudapati H. Evaluation of bioprinter technologies. Addit Manuf 2017;13:179–200. https://doi.org/10.1016/j.addma.2016.10.003.
[17] Van Noort R. The future of dental devices is digital. Dent Mater 2012;28:3–12. https://doi.org/10.1016/j.dental.2011.10.014.
[18] Tong A, Pham QL, Abatemarco P, Mathew A, Gupta D, Iyer S, et al. Review of low-cost 3D bioprinters: state of the market and observed future trends. SLAS Technol 2021;26:333–66. https://doi.org/10.1177/24726303211020297.
[19] Xu P, Guo W, Yang L, Yang C, Ruan D, Xu J, et al. Crashworthiness analysis of the biomimetic lotus root lattice structure. Int J Mech Sci 2024;263:108774. https://doi.org/10.1016/j.ijmecsci.2023.108774.
[20] Todd EA, Mirsky NA, Silva BLG, Shinde AR, Arakelians ARL, Nayak VV, et al. Functional scaffolds for bone tissue regeneration: a comprehensive review of materials, methods, and future directions. J Funct Biomater 2024;15. https://doi.org/10.3390/jfb15100280.
[21] Girija M, Kumar TS. A comparative investigation on the development of porous-structured Akermanite (Ca2MgSi2O7) via ball milling, sol–gel, and combination (hybrid) process for orthopedic applications. J Mater Res 2024;39:2198–214. https://doi.org/10.1557/s43578-024-01378-6.
[22] Montalbano G, Calore AR, Vitale-Brovarone C. Extrusion 3D printing of a multiphase collagen-based material: an optimized strategy to obtain biomimetic scaffolds with high shape fidelity. J Appl Polym Sci 2023;140:1–14. https://doi.org/10.1002/app.53593.
[23] Standard ISO. 5833: 2002; implants for Surgery—Acrylic resin cements. Geneva, Switzerland: International Standards Organization; 2002.
[24] Harun NH, Rabiatul RB, Noordin SS, Sreekantan S, Saharuddin KA, Basiron N. Hemocompatibility profiles of LLDPE with TiO2/ZnO nanocomposites for biomedical application according to ISO 10993-4 and ASTM 756-00 (2000) Guidelines. BioNanoScience 2023;13:2195–204. https://doi.org/10.1007/s12668-023-01182-2.
[25] Henkelman S, Rakhorst G, Blanton J, van Oeveren W. Standardization of incubation conditions for hemolysis testing of biomaterials. Mater Sci Eng C 2009;29:1650–4. https://doi.org/10.1016/j.msec.2009.01.002.
[26] Kokubo T, Takadama H. How useful is SBF in predicting in vivo bone bioactivity? Biomaterials 2006;27:2907–15. https://doi.org/10.1016/j.biomaterials.2006.01.017.
[27] Buj-Corral I, Bagheri A, Sivatte-Adroer M. Effect of printing parameters on dimensional error, surface roughness and porosity of FFF printed parts with grid structure. Polymers 2021;13. https://doi.org/10.3390/polym13081213.
[28] Maynard SA, Winter CW, Cunnane EM, Stevens MM. Advancing cell-instructive biomaterials through increased understanding of cell receptor spacing and material surface functionalization. Regen Eng Transl Med 2021;7:533–47. https://doi.org/10.1007/s40883-020-00180-0.
[29] Zhu G, Wang G, Li JJ. Advances in implant surface modifications to improve osseointegration. Mater Adv 2021;2:6901–27. https://doi.org/10.1039/d1ma00675d.
[30] Picado-Tejero D, Mendoza-Cerezo L, Rodríguez-Rego JM, Carrasco-Amador JP, Marcos-Romero AC. Recent advances in 3D bioprinting of porous scaffolds for tissue engineering: a narrative and critical review. J Funct Biomater 2025;16. https://doi.org/10.3390/jfb16090328.
[31] Haja Hameed AS, Karthikeyan C, Senthil Kumar V, Kumaresan S, Sasikumar S. Effect of Mg2 +, Ca2 +, Sr2 + and Ba2 + metal ions on the antifungal activity of ZnO nanoparticles tested against Candida albicans. Mater Sci Eng C 2015;52:171–7. https://doi.org/10.1016/j.msec.2015.03.030.
[32] Tabassum N, Kumar D, Verma D, Bohara RA, Singh MP. Zirconium oxide (ZrO2) nanoparticles from antibacterial activity to cytotoxicity: a next-generation of multifunctional nanoparticles. Mater Today Commun 2021;26. https://doi.org/10.1016/j.mtcomm.2021.102156.
[33] Harun NH, Smn Mydin RB, Noordin SS, Sreekantan S, Saharuddin KA, Basiron N. Hemocompatibility profiles of LLDPE with TiO2/ZnO nanocomposites for biomedical application according to ISO 10993-4 and ASTM 756-00 (2000) guidelines. BioNanoScience 2023;13:2195–204.
[34] Kang YJ, Serhrouchni S, Makhro A, Bogdanova A, Lee SS. Simple assessment of red blood cell deformability using blood pressure in capillary channels for effective detection of subpopulations in red blood cells. ACS Omega 2022;7:38576–88. https://doi.org/10.1021/acsomega.2c04027.
[35] Kothandam S, Selvatharani V, Vijayakumar N, Alex RA, Abraham J, Maheshwaran S, et al. Zinc doped akermanite: a promising biomaterial for orthopedic application with enhanced bioactivity, mechanical strength, and bacterial Study. ACS Omega 2025;10:1911–26. https://doi.org/10.1021/acsomega.4c05482.